



## Physical, electrical and magnetic properties of nano-sized Co-Cr substituted magnesium ferrites

Muhammad Javed Iqbal, Zahoor Ahmad, Turgut Meydan, and Yevgen Melikhov

Citation: *J. Appl. Phys.* **111**, 033906 (2012); doi: 10.1063/1.3676438

View online: <http://dx.doi.org/10.1063/1.3676438>

View Table of Contents: <http://jap.aip.org/resource/1/JAPIAU/v111/i3>

Published by the [American Institute of Physics](http://www.aip.org).

---

### Related Articles

Searching for high-k RE<sub>2</sub>O<sub>3</sub> nanoparticles embedded in SiO<sub>2</sub> glass matrix

*J. Appl. Phys.* **111**, 064103 (2012)

Effects of alignment, pH, surfactant, and solvent on heat transfer nanofluids containing Fe<sub>2</sub>O<sub>3</sub> and CuO nanoparticles

*J. Appl. Phys.* **111**, 064308 (2012)

Size effect on the structural, magnetic, and magnetotransport properties of electron doped manganite La<sub>0.15</sub>Ca<sub>0.85</sub>MnO<sub>3</sub>

*J. Appl. Phys.* **111**, 07D729 (2012)

Determination of spin-dependent Seebeck coefficients of CoFeB/MgO/CoFeB magnetic tunnel junction nanopillars

*J. Appl. Phys.* **111**, 07C520 (2012)

Effect of packing fraction on ferromagnetic resonance in NiFe<sub>2</sub>O<sub>4</sub> nanocomposites

*J. Appl. Phys.* **111**, 07E348 (2012)

---

### Additional information on *J. Appl. Phys.*

Journal Homepage: <http://jap.aip.org/>

Journal Information: [http://jap.aip.org/about/about\\_the\\_journal](http://jap.aip.org/about/about_the_journal)

Top downloads: [http://jap.aip.org/features/most\\_downloaded](http://jap.aip.org/features/most_downloaded)

Information for Authors: <http://jap.aip.org/authors>

### ADVERTISEMENT



**FIND THE NEEDLE IN THE  
HIRING HAYSTACK**

Post jobs and reach  
thousands of hard-to-find  
scientists with specific skills



<http://careers.physicstoday.org/post.cfm> **physicstoday JOBS**

## Physical, electrical and magnetic properties of nano-sized Co-Cr substituted magnesium ferrites

Muhammad Javed Iqbal,<sup>1,a)</sup> Zahoor Ahmad,<sup>1</sup> Turgut Meydan,<sup>2</sup> and Yevgen Melikhov<sup>2</sup>

<sup>1</sup>Surface and Solid State Chemistry Laboratory, Department of Chemistry, Quaid-i-Azam University, Islamabad 45320, Pakistan

<sup>2</sup>Wolfson Centre for Magnetism, School of Engineering, Cardiff University, Cardiff CF24 3AA, United Kingdom

(Received 26 February 2011; accepted 15 October 2011; published online 6 February 2012)

Co-Cr substituted magnesium ferrite nanomaterials ( $\text{Mg}_{1-x}\text{Co}_x\text{Cr}_x\text{Fe}_{2-x}\text{O}_4$  with  $x = 0.0-0.5$ ) have been prepared by the polyethylene glycol assisted micro emulsion method. X-ray diffraction analysis confirms the single-phase cubic close-packed lattice formation of synthesized materials. Hysteresis loops are measured up to field of 4 MA/m and high field region of these loops are modeled using the Law of Approach to saturation to calculate the magnetocrystalline anisotropy constant. The saturation magnetization of the samples increases initially from 148 kA/m for  $x = 0.0$  to 299 kA/m ( $x = 0.3$ ) and then decreases to 187 kA/m ( $x = 0.5$ ). Curie temperature for this series is found to be in the range of 618-766 K. Room temperature resistivity increases gradually from  $7.5 \times 10^8 \Omega\text{cm}$  ( $x = 0.0$ ) to  $3.47 \times 10^9 \Omega\text{cm}$  ( $x = 0.5$ ). Additionally, dielectric measurements are carried out at room temperature in a frequency range of 100 Hz to 3 MHz. With improvement in the values of the above-mentioned properties, the synthesized materials could be suitable for potential application in some magnetic and microwave devices. © 2012 American Institute of Physics. [doi:10.1063/1.3676438]

### I. INTRODUCTION

Magnetic materials, particularly nano sized ferrites show a significant change in physical, electrical, and magnetic properties in contrast to their bulk counterparts due to their high surface to volume ratio of the grains. Nanocrystalline spinel ferrites of general formula,  $\text{MFe}_2\text{O}_4$  ( $\text{M} = \text{Mg}^{2+}$ ,  $\text{Zn}^{2+}$ ,  $\text{Co}^{2+}$ ,  $\text{Cu}^{2+}$ , etc.) are currently used as key materials for the advancements in information storage systems, ferrofluid technology, magnetic refrigeration, detoxification of biological fluids, magnetic resonance imaging (MRI) contrast enhancement, and magnetic cell separation.<sup>1,2</sup>

Nanoparticles of magnesium ferrite ( $\text{MgFe}_2\text{O}_4$ ) are the potential candidate for various applications due to their high electrical resistivity, low magnetic and dielectric losses.<sup>3,4</sup> These applications include usage in microwave control components and electronic device components such as high frequency (HF) antenna design, transformers, etc.

Properties of ferrite materials are strongly influenced by the distribution of metallic ions among crystallographic crystal lattice sites that in turn is sensitive to the method used to prepare that materials.<sup>5</sup> Study of dc-electrical, dielectric and magnetic properties of ferrite materials provides valuable information about the conduction mechanism and magnetic state of the ions. Doping of  $\text{MgFe}_2\text{O}_4$  with one or several metals to alter its properties is considered the best method to modify the properties of ferrites, as was done recently with Cr<sup>6</sup> and Ca.<sup>7</sup> However, studies on doping with metallic binary mixture at iron and magnesium sites have been rarely reported. In addition, a little information is available about

the nanosized ferrites formed by the polyethylene glycol (PEG) assisted microemulsion method.

In this study, we prepared nanosized  $\text{Mg}_{1-x}\text{Co}_x\text{Cr}_x\text{Fe}_{2-x}\text{O}_4$  compounds containing different levels of Co-Cr ( $x = 0.0-0.5$ ), with the assumption that the magnetic, electrical and dielectric properties would be improved by substitution of  $\text{Mg}^{2+}$  and  $\text{Fe}^{3+}$  with  $\text{Co}^{2+}$  and  $\text{Cr}^{3+}$  ions. The presence of  $\text{Co}^{2+}$  could improve the magnetic properties. Moreover, substitution of magnesium ferrites with  $\text{Cr}^{3+}$  at the B-site should be effective in enhancing the electrical resistivity. In the present work, the aim of  $\text{Cr}^{3+}$  substitution combined with  $\text{Co}^{2+}$  is to maintain the overall electroneutrality, to reduce dielectric loss and to improve dc-electrical resistivity and magnetic properties.

### II. EXPERIMENTAL

The chemicals used in the synthesis of samples were  $\text{Mg}(\text{NO}_3)_2 \cdot 6\text{H}_2\text{O}$  (Merck, 99.9%),  $\text{Co}(\text{CH}_3\text{COO})_2$  (Fluka, 99.0%),  $\text{Fe}(\text{NO}_3)_3 \cdot 9\text{H}_2\text{O}$  (Merck, 99.0%),  $\text{Cr}(\text{NO}_3)_3$  (Reidal, 99.0%), Polyethylene glycol (BDH chemicals) and ammonia solution (Fluka, 33%). All of these chemicals were of analytical purity and therefore used as received. Magnesium ferrite samples doped simultaneously with Co and Cr, ( $\text{Mg}_{1-x}\text{Co}_x\text{Cr}_x\text{Fe}_{2-x}\text{O}_4$  where  $x = 0.0-0.5$ ) were prepared by PEG assisted microemulsion method with the details of the procedure given below.

Aqueous solutions of magnesium nitrate, cobalt acetate, iron nitrate, and chromium nitrate in a molar ratio 1: 2 of divalent ( $\text{Mg}^{2+}/\text{Co}^{2+}$ ) to trivalent ( $\text{Fe}^{3+}/\text{Cr}^{3+}$ ) metal cations, were mixed with aqueous solution of PEG in ratio 0.5 of mixed metal salts/PEG. Ammonium hydroxide solution was added drop wise with constant stirring to attain pH

<sup>a)</sup>Author to whom correspondence should be addressed. Electronic mail: mjiqauchem@yahoo.com.

9–10 at which precipitation occurred. The solution was then aged overnight at room temperature. Afterwards, the solution was filtered to collect precipitates. In order to remove the excess ammonia, PEG,<sup>8</sup> and traces of any un-reacted species, the collected precipitates were washed repeatedly with de-ionized water and ethanol until pH came down to  $\sim 7$ . The precipitates were heated at a temperature of 403 K till dryness, followed by its calcination at 573 K for 2 h. Finally, the powdered material was annealed at 1123 K for 8 h with a heating rate 5 K/min to obtain the pure spinel phase.

X-Ray diffraction (XRD) analysis was performed to identify the phase formation, lattice type and for the measurement of the cell dimensions and crystallite size of the prepared ferrite materials by PANalytical 3040/60 X' Pert PRO diffractometer (Cu K $\alpha$  radiation). The patterns were recorded at  $2\theta$  in the range of  $20^\circ$ – $80^\circ$  with a scan step of  $0.04^\circ$  and scan speed of 1 step/s. SEM analysis (Hitachi S-3400 N) was performed to assess the morphological features by using the disk shaped pellets of the materials. The elemental composition was estimated by means of energy dispersive X-ray fluorescence (ED-XRF) spectrometer (Horiba, MESA-500).

The Curie temperature,  $T_C$ , was determined from a plot of normalized moment versus temperature using a vibrating sample magnetometer (VSM, model 7400 Lake Shore, USA). The M-H loops were measured using a superconducting quantum interference device (SQUID) magnetometer under an applied field of  $\pm 4$  MA/m. The first-order cubic anisotropy constant ( $K_I$ ) of the samples were determined using the Law of Approach to saturation.<sup>9</sup> The Law of Approach is said to be valid in the range  $0.97M_S < M \leq M_S$ .<sup>10</sup> Therefore, the high field region of the magnetization curve corresponding to this range was used to determine anisotropy constant,  $K_I$ .

The pellets of 13 mm diameter and 2 mm thickness were used to measure the dc-electrical resistivity by using the laboratory built two-point probe setup in a temperature range of 298–673 K. Detailed investigation of the effects of composition variation and frequency dependence of the dielectric constant ( $\epsilon'$ ) and dielectric loss tangent ( $\tan \delta$ ) were undertaken in the frequency range of 100 Hz–3 MHz using the LCR meter bridge (Wayne Kerr LCR 4275).

### III. RESULTS AND DISCUSSION

#### A. Structural and morphological properties

XRD patterns of powdered samples of  $Mg_{1-x}Co_xCr_xFe_{2-x}O_4$  ( $x = 0.0$ – $0.5$ ) are illustrated in Fig. 1. The diffraction peaks closely correspond to the standard pattern (Fig. 1, ICSD Ref. No. 01-073-1720) of a spinel magnesium ferrite with CCP structure. Lattice constant ( $a$ ), cell volume ( $V_{cell}$ ), crystallite size ( $D$ ), X-ray density ( $d_x$ ), and porosity ( $P$ ) calculated from the XRD data, are listed in Table I. The lattice constant ( $a$ ) and cell volume ( $V_{cell}$ ) are decreased slightly with the increase in dopant (Co-Cr) contents. This is due to the slight difference in ionic size of  $Fe^{3+}$  (0.64 Å) and substituent  $Cr^{3+}$  (0.63 Å), while, ionic size of  $Co^{2+}$  (0.72 Å) is comparable to that of  $Mg^{2+}$  (0.72 Å) and have no influence

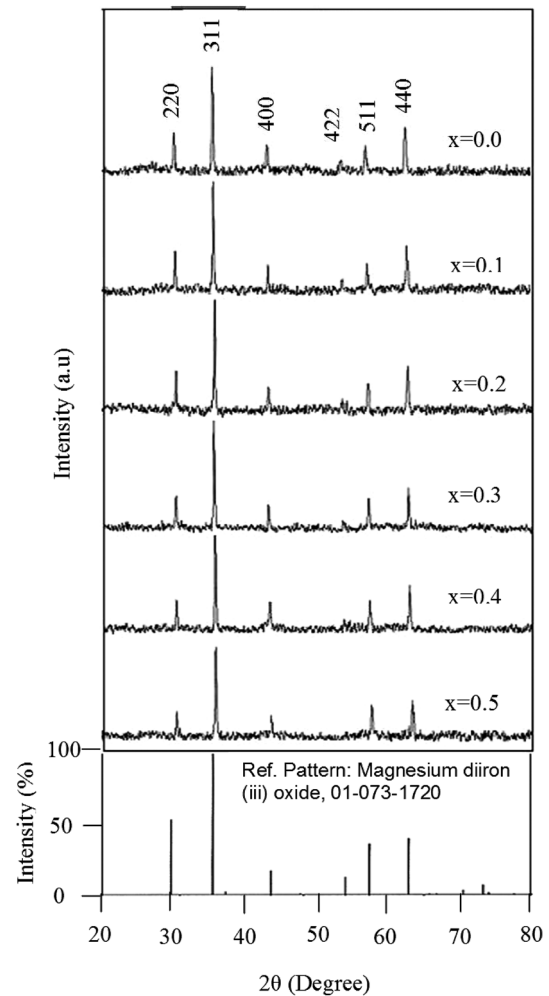


FIG. 1. XRD patterns of  $Mg_{1-x}Co_xCr_xFe_{2-x}O_4$  ( $x = 0.0$ – $0.5$ ).

on the lattice parameters. Crystallite size ( $D$ ), calculated by the well-known Scherrer formula,<sup>11</sup> is found to be in the range 23–47 nm (Table I), with the significant decrease of  $\sim 24$  nm in response to the increase in Co-Cr substitution level from  $x = 0.0$  to 0.4. The value of X-ray density ( $d_x$ ) is calculated using the following formula:

$$d_x = \frac{8M_W}{N_A V_{cell}}, \quad (1)$$

where  $M_W$  is the molar mass of the sample,  $N_A$  is the Avogadro's number, and  $V_{cell}$  is the unit cell volume. The value of  $d_x$  increases from 4.50 to 4.87 g/cm<sup>3</sup> with the increase in

TABLE I. Crystallite size ( $D$ ), lattice constant ( $a$ ), cell volume ( $V_{cell}$ ), X-ray density ( $d_x$ ), bulk density ( $d_b$ ), and porosity ( $P$ ) of  $Mg_{1-x}Co_xCr_xFe_{2-x}O_4$  ( $x = 0.0$ – $0.5$ ).

Parameters	$x = 0.0$	$x = 0.1$	$x = 0.2$	$x = 0.3$	$x = 0.4$	$x = 0.5$
$D$ (nm)	47	40	30	35	23	28
$a$ (Å)	8.384	8.380	8.380	8.379	8.378	8.379
$V_{cell}$ (Å <sup>3</sup> )	589.3	588.5	588.5	588.3	588.1	588.3
$d_x$ (g/cm <sup>3</sup> )	4.50	4.59	4.66	4.73	4.80	4.87
$d_b$ (g/cm <sup>3</sup> )	3.93	4.04	4.11	4.17	4.24	4.31
$P$ (%)	12.7	12.0	11.8	11.8	11.7	11.5

Co-Cr contents due to larger molar mass of the doped metal cations as shown in Table I. Bulk density ( $d_b$ ) of the samples is calculated from the following relation:

$$d_b = \frac{m}{\pi r^2 h}, \quad (2)$$

where  $m$ ,  $r$ , and  $h$  are mass, radius, and thickness of the pellet of sample, respectively. Data of the Table I show that for the synthesized samples in present studies, the magnitude of the bulk density,  $d_b$  is smaller than that of the  $d_x$  ( $d_b$  is  $\sim 88\%$  of  $d_x$ ) as anticipated due to some unavoidable pores created during sintering. Porosity of the samples is estimated to be in the range of 11.5%–12.7%.

The surface and grain morphology of spinel magnesium ferrite and its derivatives is studied by scanning electron microscopy (SEM). The micrographs (Figs. 2(a)–2(b)) of two representative samples of  $\text{Mg}_{1-x}\text{Co}_x\text{Cr}_x\text{Fe}_{2-x}\text{O}_4$  containing the dopant contents of  $x = 0.0$  and  $0.4$ , depict that the surface is less smooth and is a mixture of individual particles. The shaded areas in the micrographs are due to voids. The white spots show that the material is not homogeneous but as the substitution level is increased, the average size of crystallites decreases, and the material becomes homogeneous. Some of the particles shown in SEM micrographs represent the aggregates formed as a result of the agglomeration of the individual crystallites that are expected to occur at high temperature of annealing.

Elemental compositions of some representative samples of the synthesized materials are determined by ED-XRF. The observed values of the molar ratios of different components present in the samples are in close agreement with the nominal compositions as shown in Table II. It was not possible to identify the amount of oxygen with the current method and, therefore, it was assumed to be the same as that of the chemical formula.

## B. Magnetic properties

The Curie temperature ( $T_C$ ) is determined out of the magnetization temperature curve measured at low magnetic field ( $\sim 400$  kA/m). Figure 3 shows variation of the normalized moment of  $\text{Mg}_{1-x}\text{Co}_x\text{Cr}_x\text{Fe}_{2-x}\text{O}_4$  with temperature slowly decreasing. The value of  $T_C$  represents the characteristic magnetic interactions and overall strength of the exchange interactions between the spins of the cations (A-B exchange interactions) present at the two sites (A- and B-sites). The Curie temperature ( $T_C$ ) reached to a maximum

TABLE II. The observed and theoretical elemental composition values ( $\text{mol L}^{-1}$ ) of some representative samples of  $\text{Mg}_{1-x}\text{Co}_x\text{Cr}_x\text{Fe}_{2-x}\text{O}_4$  ( $x = 0.0, 0.2, \text{ and } 0.4$ ).

Theoretical values	Observed values ( $\text{mol L}^{-1}$ )			
	Mg	Co	Cr	Fe
$\text{MgFe}_2\text{O}_4$	0.97	...	...	2.02
$\text{Mg}_{0.8}\text{Co}_{0.2}\text{Cr}_{0.2}\text{Fe}_{1.8}\text{O}_4$	0.76	0.2	0.19	1.83
$\text{Mg}_{0.6}\text{Co}_{0.4}\text{Cr}_{0.4}\text{Fe}_{1.6}\text{O}_4$	0.58	0.38	0.38	1.61

value of 766 K for  $x = 0.2$  from 681 K for  $x = 0.0$ , and then decreased for  $x \geq 0.3$  (Table III). This could occur due to some modification in A-B super-exchange interaction on the behalf of substitution with Co-Cr. Videlicet, the increase in the  $T_C$  value up to the maximum value is due to replacement of non-magnetic  $\text{Mg}^{2+}$  ion ( $0 \mu_B$ ) by a magnetic  $\text{Co}^{2+}$  ion ( $3 \mu_B$ ), that would strengthen the A-B super-exchange interaction, since  $\text{Co}^{2+}$  ions are well known to produce large induced anisotropy owing to their relatively high orbital contribution to the magnetic moment.<sup>12</sup> The decrease in the  $T_C$  value above the specific level with  $x > 0.2$ , might be due to higher content of less magnetic  $\text{Cr}^{3+}$  ( $3 \mu_B$ ) ions replacing more magnetic  $\text{Fe}^{3+}$  ( $5 \mu_B$ ) ions that in turn could be responsible for the weakening of the A-B super-exchange interactions.

The high-field region of the hysteresis loops (Fig. 4) are modeled using the Law of Approach to saturation based on the assumption that at sufficiently high field only rotational processes remain, with an additional forced magnetization term that is linear with applied field. In order to evaluate the composition dependence of the anisotropy, it is assumed that all irreversible hysteretic processes are completed when the major hysteresis loop closed and that further increase of the magnetic moment is due to rotational processes which are connected with the magnetic anisotropy. Based on the Law of Approach (LoA) to saturation, which describes the dependence of magnetization,  $M$  on the applied field for  $H \gg H_C$ , magnetization near the saturation magnetization,  $M_S$  can be experimentally obtained<sup>13</sup> as

$$M = M_S \left( 1 - \frac{a}{H} - \frac{b}{H^2} - \dots \right) + \kappa H, \quad (3)$$

where  $M_S$  and  $H$  are the saturation magnetization and applied field, respectively, and  $\kappa H$  is the forced magnetization term.<sup>14</sup> The coefficient  $a \approx 0$  in the high field region as it is

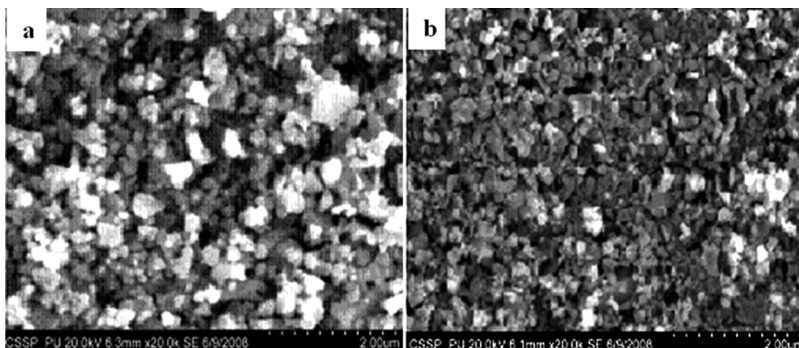


FIG. 2. SEM photographs of  $\text{Mg}_{1-x}\text{Co}_x\text{Cr}_x\text{Fe}_{2-x}\text{O}_4$  where (a)  $x = 0.0$  and (b)  $x = 0.4$ .

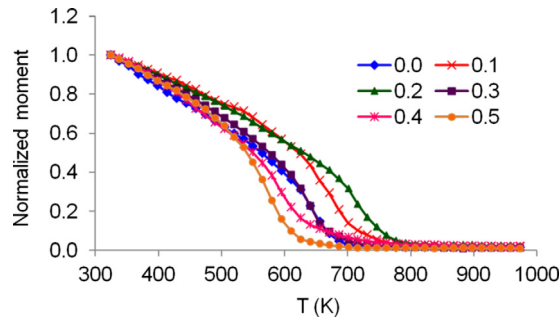


FIG. 3. (Color online) Thermal variation of normalized moment of  $\text{Mg}_{1-x}\text{Co}_x\text{Cr}_x\text{Fe}_{2-x}\text{O}_4$  ( $x = 0.0-0.5$ ).

related to domain wall pinning. For cubic structured randomly oriented polycrystalline material, the coefficient  $b$  is given by Eq. (4);<sup>15</sup>

$$b = \frac{8}{105} \frac{K_1^2}{\mu_0^2 M_S^2}. \quad (4)$$

The numerical coefficient  $8/105$  is for random polycrystalline specimens with cubic anisotropy,  $\mu_0$  is the permeability of free space, and  $K_1$  is the cubic anisotropy constant. The high-field regime of the major hysteresis curves are fitted using the standard *LoA* approach by Eqs. (3) and (4). Detailed examination of the curves revealed that forced magnetization ( $\kappa H$ ) is negligible in this regime, as might be expected. Therefore,  $\kappa = 0$  and consequently  $M_S$  and  $K_1$  are the only fitting parameters.

The composition dependence of the calculated anisotropy constant,  $K_1$  for different Co-Cr contents is shown in Table III. It is found that anisotropy constant increases substantially with increasing Co-Cr contents for the specimen with  $x \leq 0.3$ , and decreases for higher Co-Cr contents. The magnitude of anisotropy constant of  $\text{Mg}_{1-x}\text{Co}_x\text{Cr}_x\text{Fe}_{2-x}\text{O}_4$  is found to be in the range  $2.31 \times 10^5 - 4.04 \times 10^5 \text{ J/m}^3$ .

According to the one-ion model, the presence of  $\text{Co}^{2+}$  ions on the octahedral sites of the spinel structure enhances the anisotropy of ferrites.<sup>16</sup> The results of our current studies of the Co-Cr substituted magnesium ferrites suggest that in co-substituting  $\text{Co}^{2+}$  and  $\text{Cr}^{3+}$  for magnesium and iron,  $\text{Co}^{2+}$  and  $\text{Cr}^{3+}$  both go into the octahedral sites. This

TABLE III. Curie temperature ( $T_C$ ), saturation magnetization ( $M_S$ ), anisotropy constant ( $K_1$ ), remanence ( $M_r$ ), coercivity ( $H_C$ ), room temperature resistivity ( $\rho^{RT}$ ), activation energy ( $E_a$ ), dielectric constant ( $\epsilon$ ), and dielectric loss tangent ( $\tan \delta$ ) at 10 kHz, of  $\text{Mg}_{1-x}\text{Co}_x\text{Cr}_x\text{Fe}_{2-x}\text{O}_4$  ( $x = 0.0-0.5$ ).

Parameters	$x = 0.0$	$x = 0.1$	$x = 0.2$	$x = 0.3$	$x = 0.4$	$x = 0.5$
$T_C$ (K)	681	727	766	682	660	618
$M_S$ (kA/m) @ 300 K	148	169	218	299	258	187
$K_1$ ( $\text{J/m}^3$ ) $10^5$	2.31	2.77	3.79	4.04	3.02	2.51
$M_r$ (kA/m)	26	51	84	85	85	58
$H_C$ (kA/m)	4.51	21.88	27.33	21.07	20.86	12.86
$\rho^{RT}$ ( $\Omega\text{cm}$ ) $10^9$	0.75	1.48	2.14	3.02	3.39	3.47
$E_a$ (eV)	0.35	0.41	0.47	0.53	0.57	0.58
$\epsilon$ @ 10 kHz	564	457	303	109	98	96
$\tan \delta$ @ 10 kHz	0.99	0.66	0.58	0.51	0.51	0.55

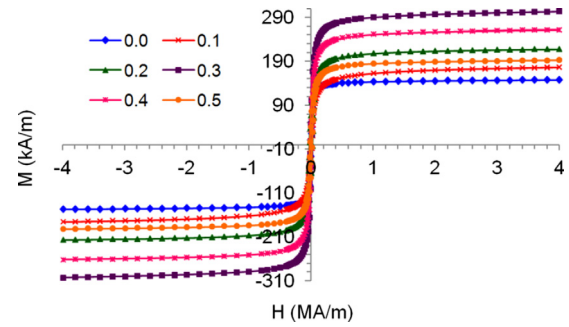


FIG. 4. (Color online) M-H loops of  $\text{Mg}_{1-x}\text{Co}_x\text{Cr}_x\text{Fe}_{2-x}\text{O}_4$  ( $x = 0.0-0.5$ ).

supports the observed increase in anisotropy with increasing  $\text{Co}^{2+}$  content to a certain specimen level. Thereafter, the observed decrease in anisotropy of  $\text{Mg}_{1-x}\text{Co}_x\text{Cr}_x\text{Fe}_{2-x}\text{O}_4$  with Co-Cr content  $x \geq 0.4$  can be interpreted in terms of the effects of  $\text{Cr}^{3+}$  substitution on site occupancies of the cations. As replacement of  $\text{Fe}^{3+}$  with  $\text{Cr}^{3+}$  at the octahedral site for higher specimen level, nullify the  $\text{Co}^{2+}$  ions contents and become effective in reducing magneto crystalline anisotropy.

The value of saturation magnetization,  $M_S$  computed by fitting Eqs. (3) and (4) to experimental data are found to be approximately the same as the measured maximum magnetization values at 4 MA/m. Saturation magnetization ( $M_S$ ), remanence ( $M_r$ ), and coercivity ( $H_C$ ) values are listed in Table III. At first, on addition of Co-Cr content, the  $M_S$  value increases from 148 kA/m ( $x = 0.0$ ) to 299 kA/m ( $x = 0.3$ ), but then it decreases for higher level of substitution. Remanence value (26–85 kA/m) varies with Co-Cr concentration in a way similar to  $M_S$  values. This enhancement of  $M_S$  is about 50% higher as compared to that reported previously by other researchers.<sup>5,7,17</sup> This observed increase in  $M_S$  value can be interpreted in terms of the effects of cation distribution into A- and B-sites. The net magnetism of the spinel ferrite is due to the presence of uncompensated electron spins of the individual magnetic ions and anti-parallel spin alignment in the two (A and B) sublattices of the spinel structure.<sup>18</sup> Magnesium ferrite ( $\text{MgFe}_2\text{O}_4$ ) is a partially inverted spinel ferrite, i.e.,  $(\text{Mg}_{1-\lambda}\text{Fe}_\lambda)[\text{Mg}_\lambda\text{Fe}_{2-\lambda}]\text{O}_4$  where parenthesis and square brackets denote cation sites of tetrahedral (A-sites) and octahedral (B-sites) coordination, respectively.<sup>19</sup>  $\text{Mg}^{2+}$  is a non-magnetic ion and has no contribution in the magnetic moment of  $\text{MgFe}_2\text{O}_4$ , which is thus entirely due to the uncompensated spins of the un-evenly distributed iron ions at two (A and B) sites.

In the present study, simultaneous substitution of  $\text{Co}^{2+}$  and  $\text{Cr}^{3+}$  to replace  $\text{Mg}^{2+}$  and  $\text{Fe}^{3+}$  has brought in quite significant variation in magnetic properties. In this quaternary system, Mg and Fe ions are partially distributed over both A- and B-sites while Cr ions are known for strong preference to the B-site.<sup>20</sup> Co ions usually prefer B-site but not always as it depend upon different factors like preparation method, annealing temperature and doping concentration, etc. Replacement of non-magnetic  $\text{Mg}^{2+}$  ion by magnetic ( $\text{Co}^{2+}$ ) ion would help to enhance the magnetic moment of B-site leading to an increase in the net magnetic moment. On the

other hand, substitution of  $\text{Fe}^{3+}$  ( $5 \mu_B$ ) by less magnetic  $\text{Cr}^{3+}$  ( $3 \mu_B$ ) would result in dilution of magnetization on the same site. Hence, this might cause an interesting competition between two ions at the same site, leading to an increase in the value of  $M_S$  to certain specimen level and starts to decrease afterwards. However, the overall effect of Co-Cr substitution is to increase  $M_S$  value to acceptable figure for different magnetic applications.

With an increase in Co-Cr level of  $\text{MgFe}_2\text{O}_4$ , coercivity increases initially to dopant content,  $x=0.2$  and start to decrease for higher level of substitution as shown in Table III. This decreasing trend might be due to the decrease in magneto crystalline anisotropy.

The Co-Cr doped magnesium ferrite nanomaterials synthesized in the present work are found to have high saturation magnetization (max  $\sim 299$  kA/m) and moderate coercivity value (4.51–27.33 kA/m) and, therefore, may be considered attractive materials for certain applications. For example, despite gradual leaning toward perpendicular recording media where high saturation magnetization and high coercivity is required, in case of longitudinal recording media high coercivity is avoided in order to facilitate re-recording.<sup>21</sup> The Co-Cr doped magnesium ferrite nanomaterials could serve this purpose.

### C. Electrical properties

Variation in dc-electrical resistivity ( $\rho$ ) of the synthesized samples measured in the temperature range of 298–673 K is shown in Fig. 5. This figure exhibits a rapid increase in resistivity with temperature increment (metal like behavior), followed by a linear decrease above a specific transition temperature  $T_{MS}$ . Such resistivity–temperature behavior has also been reported for Al–Cr substituted spinel ferrite.<sup>22</sup> This resistivity–temperature behavior may be attributed to several factors including the occurrence of phase transition, cations migration, cations re-ordering, presence of impurities, and the magneto-transport effect. In this case, however, there is no real possibility of any phase transition at such low temperatures (358–373 K) and the XRD data do not show the presence of any impurity phase in the samples. The cation migration is also not so fast at such low temperatures to give rise to the observed behavior but cannot be excluded. The other possible and most likely cause of the observed metallic

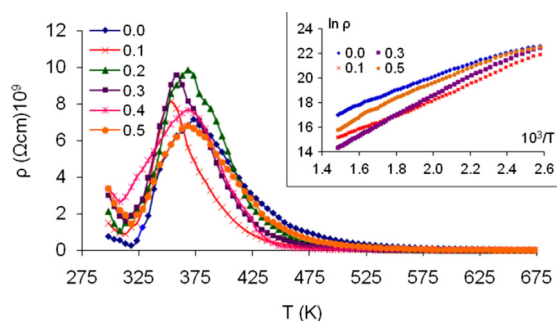
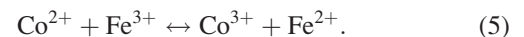


FIG. 5. (Color online) Plot of dc-electrical resistivity of  $\text{Mg}_{1-x}\text{Co}_x\text{Cr}_x\text{Fe}_{2-x}\text{O}_4$  ( $x=0.0-0.5$ ) vs temperature. Inset shows Arrhenius type plot of  $\ln \rho$  vs  $1000/T$  for representative samples of Co-Cr doped magnesium ferrite.

behavior at low temperatures of  $\sim 373$  K is the absorbed water as spinel magnesium ferrites are generally hygroscopic in nature.<sup>23</sup> Although the experiments were performed in dry atmosphere, the possibility of moisture present deep within the pores of the samples pellets cannot be ruled out.

Electrical properties of ferrites generally depend upon the composition and preparative parameters of the synthesized materials.<sup>24</sup> Electrical conduction in ferrite nanomaterials is due to electronic hopping between ion pairs of the same type of element on equivalent sublattice sites but having different valence state. The number of such ion pairs depends upon the sintering conditions and extent of reduction of  $\text{Fe}^{3+}$  to  $\text{Fe}^{2+}$  at elevated temperature.  $\text{Fe}^{2+}/\text{Fe}^{3+}$  ratio on the B-sites controls the overall resistivity in ferrites materials. Room temperature resistivity ( $\rho^{RT}$ ) of magnesium ferrite samples increases from a value of  $7.50 \times 10^8$ – $3.47 \times 10^9$   $\Omega$  cm by doping with different contents of Co-Cr binary mixture (Table III). A sharp and significant increase in resistivity for low levels of the dopants is quite noticeable while the increase is less pronounced for higher concentration (Fig. 6). Spinel ferrites have been previously doped with  $\text{Ca}^{2+}$ ,<sup>25</sup>  $\text{Zn}^{2+}$ ,<sup>26</sup>  $\text{Zr-Mn}$ ,<sup>27</sup>  $\text{Co-Ni}$ ,<sup>28</sup> and  $\text{Zr-Ni}$ ,<sup>29</sup> and their room temperature resistivity is found to be in the range of  $10^6$ – $10^7$   $\Omega$  cm which is  $\sim 100$  times less than that achieved in this study. So, Co-Cr doped materials can be suitable to curb the eddy current losses for microwave applications. However, direct magnetic loss measurements in a wide frequency range and their complete analysis,<sup>30</sup> are required to fully address the applicability of Co-Cr doped materials for microwave applications; we plan to do this study elsewhere.

Variation in resistivity with dopant concentration is explained based on occupancy of cations in the sub-lattices of the spinel structure. The conduction in magnesium ferrite is due to transfer of electrons between  $\text{Fe}^{2+}$  and  $\text{Fe}^{3+}$  ions. In Co-Cr doped samples, substitution of  $\text{Cr}^{3+}$  for  $\text{Fe}^{3+}$  results in a decrease of  $\text{Fe}^{3+}$  ions at B-site (which are in fact responsible for hopping). However, substitution of  $\text{Co}^{2+}$  at the B-site might generate holes by the following exchange reaction, which can also be involved in conduction:



The electron hopping however, would mainly contribute in conduction and the overall effect of doping of binary mixture of Co-Cr is to increase in resistivity.

In ferrites, the electrons are localized and an overlap between the wave functions of ions situated on adjacent sites is small. The electron mobility is temperature dependent and

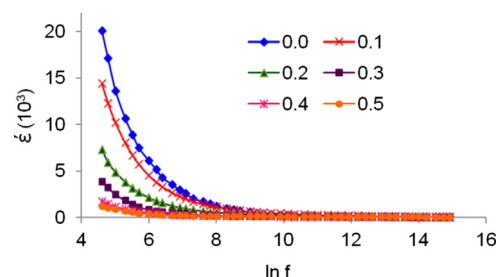


FIG. 6. (Color online) Dielectric constant ( $\epsilon$ ) of  $\text{Mg}_{1-x}\text{Co}_x\text{Cr}_x\text{Fe}_{2-x}\text{O}_4$  ( $x=0.0-0.5$ ) vs  $\ln f$ .

is characterized by activation energy. The activation energy in the present case is obtained by fitting the dc-resistivity data to the Arrhenius relation,

$$\rho = \rho^{\circ} \exp\left(\frac{E_a}{k_B T}\right), \quad (6)$$

where  $E_a$  is the activation energy and  $k_B$  is the Boltzmann constant. The inset of Fig. 5 shows the variation of  $\ln \rho$  with  $10^3/T$  of some of the samples. The values of activation energy are in accordance with the resistivity data.

#### D. Dielectric properties

The variation of the real part of the dielectric constant ( $\epsilon'$ ) as a function of applied frequency at room temperature is shown in Fig. 6. The dielectric constant has been calculated in a frequency range of 100 Hz-3 MHz from the following relation:

$$\epsilon' = \frac{Cd}{\epsilon_0 A}, \quad (7)$$

where  $C$  is the capacitance of the pellet in farad,  $d$  is the thickness of the pellet in meter,  $A$  is the cross-sectional area of the flat surface of the pellet, and  $\epsilon_0$  is the permittivity constant of free space.

The dielectric constant is normally quite high but decreases rapidly with an increase in frequency in the low frequency regime, however a small decrease is observed in the high frequency region, which is normal behavior of ferrite materials. A similar variation of the dielectric constant with frequency was observed in the cases of  $\text{ZnFe}_2\text{O}_4$  and  $\text{MnFe}_2\text{O}_4$ ,<sup>31</sup>  $\text{Zn}_x\text{Cu}_{1-x}\text{Fe}_2\text{O}_4$  and  $\text{Mn}_x\text{Cu}_{1-x}\text{Fe}_2\text{O}_4$ .<sup>32</sup>

Dielectric behavior of the spinel ferrites can be explained by considering interfacial polarization due to surface effect. At low frequency, the dipolar and interfacial polarization both contribute to the value of dielectric constant but at higher frequency, only the electronic polarization becomes significant. At low frequency, the electron exchange between  $\text{Fe}^{2+}$  and  $\text{Fe}^{3+}$  ions is capable to follow the alternating field but the frequency of electron exchange between two ions cannot follow the high alternating field. This results in a decrease in polarization and the conduction lag beyond a certain frequency of externally applied field. Therefore, the value of dielectric constant is lower at high frequencies than at low frequencies. Furthermore, the dielectric properties of heterogeneous systems like ferrites are dependent on several factors including the method of preparation, sintering temperature, sintering atmosphere, etc. Since, ferrite powdered samples are sintered under slightly reducing conditions, the divalent iron  $\text{Fe}^{2+}$  is expected to be formed in the body of the ferrite material leading to high conductivity grains. When such a material is cooled in an atmosphere of oxygen, it is possible to form layers of very low conductivity over its constituent grains. Almost all the ferrites in the polycrystalline form have such high conductivity grains separated by low conductivity layers so that they behave as heterogeneous dielectric materials. Due to the het-

erogeneous dielectric behavior, dielectric constant as high as  $10^3$ - $10^5$  is observed in the case of ferrites at low frequencies.

The room temperature value of dielectric constant for different dopant concentration is observed to decrease from 564 ( $x=0.0$ ) to 96 ( $x=0.5$ ) at frequency of 10 kHz and listed in Table III. These values are  $10^2$  to  $10^3$  times smaller than those of bulk magnesium ferrite. Dube<sup>33</sup> has also observed a decrease in dielectric constant for nanoparticles by about 3%-8% compared to bulk particles (50  $\mu\text{m}$  and above). El Hiti<sup>34</sup> has obtained a value of  $10^4$  for  $\epsilon'$  at 312 K (at 1 kHz) for the bulk  $\text{MgFe}_2\text{O}_4$ . In the present studies,  $\epsilon'$  is found to be in the order of  $10^1$ - $10^2$  for the Co-Cr co-doped samples at the same temperature and 10 kHz, which is two orders of magnitude smaller than that of the bulk  $\text{MgFe}_2\text{O}_4$ . The considerably high values at low frequency can be attributed to higher capacitance of the grain boundary. It can be seen from Fig. 6 that the dispersion of  $\epsilon'$  with the frequency is maximum for undoped Mg-ferrite and magnitude of dispersion decreases as more Co-Cr is incorporated. The decrease in the value of  $\epsilon'$  with Co-Cr content is due to reduction in Fe contents to be polarized (space charge carriers) at the B-site, resulting in a low space charge polarization governed by space charge carriers and resistivity of the materials. Further, since electrical resistivity and dielectric both are transport properties whose variations are proportional to the sample composition, possibly the mechanism responsible for these two phenomena may be the same or similar to each other (see Fig. 7).

Figure 8 shows the variation of dielectric loss tangent ( $\tan \delta$ ) with frequency, at room temperature for  $\text{Mg}_{1-x}\text{Co}_x\text{Cr}_x\text{Fe}_{2-x}\text{O}_4$  samples. By an increase in frequency, the value of  $\tan \delta$  initially decreases faster than that of  $\epsilon'$  but the rate of decrease becomes closer to that of  $\epsilon'$  at high frequency range, which is normal behavior of ferrites. The value of  $\tan \delta$  depend upon a number of factors, such as stoichiometry,  $\text{Fe}^{2+}$  content, and structural homogeneity, which in turn depends upon composition and sintering temperature.<sup>35</sup> The observed decrease in  $\tan \delta$  with an increase of frequency can be explained on the basis of Koop's phenomenological theory.<sup>36</sup>

In the low frequency region, which corresponds to high resistivity (due to grain boundaries), more energy is required for electron exchange between  $\text{Fe}^{2+}$  and  $\text{Fe}^{3+}$  ions and thus energy loss is high. In the high frequency range, which corresponds to low resistivity (due to the grains), a small energy is needed for electron transfer between  $\text{Fe}^{2+}$  and  $\text{Fe}^{3+}$  ions

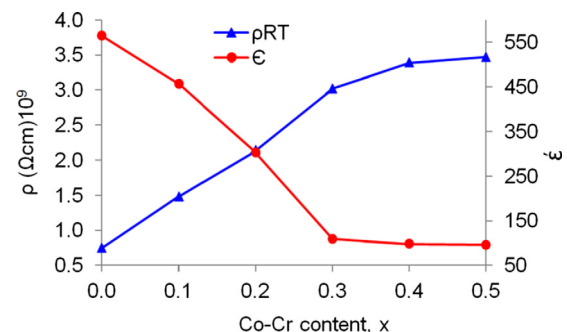


FIG. 7. (Color online) Variation of room temperature resistivity ( $\rho^{\text{RT}}$ ) and dielectric constant ( $\epsilon'$ ) with Co-Cr content for  $\text{Mg}_{1-x}\text{Co}_x\text{Cr}_x\text{Fe}_{2-x}\text{O}_4$  ( $x = 0.0-0.5$ ).

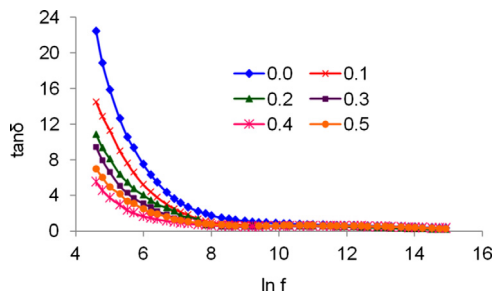


FIG. 8. (Color online) Dielectric loss tangent ( $\tan \delta$ ) of  $\text{Mg}_{1-x}\text{Co}_x\text{Cr}_x\text{Fe}_{2-x}\text{O}_4$  ( $x = 0.0-0.5$ ) vs  $\ln f$ .

in the grains and accompanied by a small eddy current and hence a decrease in the energy loss. None of the samples exhibits the loss peak. The peaking nature occurs when the jumping frequency of electrons between  $\text{Fe}^{2+}$  and  $\text{Fe}^{3+}$  is equal to the frequency of the applied ac field. All the samples show dispersion in  $\tan \delta$  in lower frequencies.

Iwauchi<sup>37</sup> has clearly established a reciprocal relationship between dielectric losses and dc-electrical resistivity. Table III shows the compositional dependence of  $\tan \delta$  at 10 kHz and found to be much smaller than that of reported for bulk magnesium ferrite. El Hiti<sup>34</sup> has obtained a value of  $10^1$  for  $\tan \delta$  at 312 K (at 1 kHz) for the bulk  $\text{MgFe}_2\text{O}_4$  prepared by ceramic method. In the present study,  $\tan \delta$  for all samples is about 0.5–1.0 at 300 K and 10 kHz. The dielectric loss is thus found to be two orders of magnitude lower compared to that of the bulk.<sup>34</sup>

#### IV. CONCLUSIONS

An attempt is made to meet the challenges for the advancements in the new ferrite technology. The PEG assisted route is a reliable and economic method to synthesize spinel single-phase and nano-crystallite magnesium ferrite with crystallite size in the range 23–47 nm. Co-substitution of Co-Cr at magnesium and iron sites in magnesium ferrite accompanies complicated effects on magnetic properties, however, produces quite significant and remarkable changes in the structural, electrical, and magnetic properties. The synthesized nanomaterials possess high saturation magnetization and moderate coercive field and may have a potential for different magnetic applications. The improvement in room temperature resistivity together with low dielectric loss indicates that Co-Cr doped Mg-ferrite can be useful for switching applications.

#### ACKNOWLEDGMENTS

The authors are grateful to the Higher Education Commission (HEC) of Pakistan for financial support, and Center

for Solid State Physics, University of the Punjab, Lahore, Pakistan for SEM analysis.

- <sup>1</sup>A. K. Giri, E. M. Kirkpartrick, P. Mongkhamllang, and S. A. Majetich, *Appl. Phys. Lett.* **80**, 2341 (2002).
- <sup>2</sup>M. F. Hansen and S. Morup, *J. Magn. Magn. Mater.* **184**, 262 (1998).
- <sup>3</sup>L. B. Kong, Z. W. Li, G. Q. Lin, and Y. B. Gan, *J. Am. Ceram. Soc.* **90**, 2104 (2007).
- <sup>4</sup>Y. Konseoglu, H. Kavas, and B. Aktas, *Phys. Status Solidi A* **203**, 1595 (2006).
- <sup>5</sup>M. M. Bahout, S. Bertrand, and O. Pena, *J. Solid State Chem.* **178**, 1080 (2005).
- <sup>6</sup>P. P. Hankare, V. T. Vader, N. M. Patil, S. D. Jadhav, U. B. Sankpal, M. R. Kadam, B. K. Chougule, and N. S. Gajbhiye, *Mater. Chem. Phys.* **113**, 233 (2009).
- <sup>7</sup>H. Hirazawa, S. Kusamoto, H. Aono, T. Naohara, K. Mori, Y. Hattori, T. Maehara, and Y. Watanabe, *J. Alloys Compd.* **461**, 467 (2008).
- <sup>8</sup>A. Kumbhar, L. Spinu, F. Agnoli, K. Y. Wang, W. Zhou, and C. J. O'Connor, *IEEE Trans. Magn.* **37**, 2216 (2001).
- <sup>9</sup>N. Ranvah, Y. Melikhov, D. C. Jiles, J. E. Snyder, A. J. Moses, P. I. Williams, and S. H. Song, *J. Appl. Phys.* **103**, 07E506 (2008).
- <sup>10</sup>E. W. Lee, *Rep. Prog. Phys.* **18**, 184 (1955).
- <sup>11</sup>M. J. Iqbal and Z. Ahmad, *J. Power Sources* **179**, 763 (2008).
- <sup>12</sup>B. S. Chauhan, R. Kumar, K. M. Jadhav, and M. Singh, *J. Magn. Magn. Mater.* **283**, 71 (2004).
- <sup>13</sup>S. Chikazumi, *Physics of Ferromagnetism*, 2nd ed. (Oxford University Press, Oxford, UK, 1997), p. 503.
- <sup>14</sup>D. Cullity, *Introduction to Magnetic Materials* (Addison-Wesley Pub. Co., Reading, MA, 1972), p. 347.
- <sup>15</sup>R. M. Bozorth, *Ferromagnetism* (IEEE Press, New York, 1993), p. 486.
- <sup>16</sup>J. C. Slonczewski, *Phys. Rev.* **110**, 1341 (1958).
- <sup>17</sup>A. Pradeep, P. Priyadharsini, and G. Chandrasekaran, *J. Magn. Magn. Mater.* **320**, 2774 (2008).
- <sup>18</sup>L. Zhao, H. Zhang, Y. Xing, S. Song, S. Yu, W. Shi, X. Guo, J. Yang, Y. Lei, and F. Cao, *J. Solid State Chem.* **181**, 245 (2008).
- <sup>19</sup>A. Franco, Jr. and M. S. Silva, *J. Appl. Phys.* **109**, 07B505 (2011).
- <sup>20</sup>N. Nanba, *J. Appl. Phys.* **49**, 2950 (1978).
- <sup>21</sup>M. M. Hessien, M. Radwan, and M. M. Rashad, *J. Anal. Appl. Pyrolysis* **78**, 282 (2007).
- <sup>22</sup>U. V. Chhaya and R. G. Kulkarni, *Mater. Lett.* **39**, 91 (1999).
- <sup>23</sup>E. Rezlescu, N. Rezlescu, and P. D. Popa, *Phys. Status Solidi* **1**, 3636 (2004).
- <sup>24</sup>S. Zahi, A. R. Daud, and M. Hashim, *Mater. Chem. Phys.* **106**, 452 (2007).
- <sup>25</sup>S. D. Chhaya, M. P. Pandya, M. C. Chhantbar, K. B. Modi, G. J. Balda, and H. H. Joshi, *J. Alloys Compd.* **377**, 155 (2004).
- <sup>26</sup>P. K. Roy and J. Bera, *J. Mater. Process. Technol.* **197**, 279 (2008).
- <sup>27</sup>M. J. Iqbal and M. R. Siddiquah, *J. Magn. Magn. Mater.* **320**, 845 (2008).
- <sup>28</sup>I. H. Gul, F. Amin, A. Z. Abbasi, M. A. Rehman, and A. Maqsood, *Scr. Mater.* **56**, 497 (2007).
- <sup>29</sup>M. N. Ashiq, S. Saleem, M. A. Malana, and A. Rehman, *J. Alloys Compd.* **486**, 640 (2009).
- <sup>30</sup>F. Fiorillo, M. Coisson, C. Beatrice, and M. Pasquale, *J. Appl. Phys.* **105**, 07A517 (2009).
- <sup>31</sup>K. Iwauchi, *Jpn. J. Appl. Phys.* **10**, 1520 (1971).
- <sup>32</sup>N. Rezlescu and E. Rezlescu, *Phys. Status Solidi A* **23**, 575 (1974).
- <sup>33</sup>D. C. Dube, *J. Phys. D: Appl. Phys.* **3**, 1648 (1970).
- <sup>34</sup>M. A. El Hiti, *J. Magn. Magn. Mater.* **192**, 305 (1999).
- <sup>35</sup>S. Dutta, R. N. P. Choudhary, and P. K. Sinha, *Phys. Status Solidi A* **202**, 1172 (2005).
- <sup>36</sup>C. G. Koops, *Phys. Rev.* **83**, 121 (1951).
- <sup>37</sup>K. Iwauchi, *Phys. Status Solidi A* **92**, 309 (1985).